Electric Power Systems Research 181 (2020) 106193

Contents lists available at ScienceDirect

Electric Power Systems Research

journal homepage: www.elsevier.com/locate/epsr

A scenario-based analytical method for probabilistic load flow analysis

Chenxu Wang[a], Chengxi Liu[a], Fei Tang[a,*], Dichen Liu[a], Yixi Zhou[b]

[a] School of Electrical Engineering and Automation, Wuhan University, Wuhan, Hubei Province, China
[b] State Grid Hangzhou Electric Power Supply Company, Hangzhou, Zhejiang Province, China

ARTICLE INFO

Keywords:
Probabilistic load flow
Renewable energy source
Correlation
Scenario analysis
Cumulant

ABSTRACT

In recent years, power system uncertainties have increased due to the growing integrations of intermittent renewable energy resources. It is imperative to introduce probabilistic load flow analysis in the study of power system operation and planning to adapt to the ever-increasing uncertainties. This paper proposes a scenario-based analytical method for the probabilistic load flow analysis, which takes advantage of both the scenario analysis method and the cumulant method. This method can not only consider various kinds of correlations among power inputs but also accurately represent the probability distributions of desired outputs with a reasonable computational burden. The performance of this method is evaluated on the IEEE 14-bus and 118-bus test systems. The accuracy and efficiency of the proposed method are validated through quantitative and graphical comparisons with Monte-Carlo simulation.

1. Introduction

In the past few years, renewable energy sources (RES) have experienced rapid development due to their numerous advantages. More and more uncertainties have been penetrating into the modern power systems, not only from load demands, network topology changes, outages of system components but also from the generations of RES, such as solar and wind power. Besides, due to complex meteorological processes, there are significant spatiotemporal correlations among the RES generation. Hence, assessing the behaviors of power systems with complex uncertainties becomes indispensable.

Probabilistic load flow (PLF), firstly proposed in 1974 [1], has become the commonly used tool to analyze the influence of power system uncertainties. There are three mainstream PLF methods: numerical methods, analytical methods, and approximate methods [2].

As the most straightforward numerical method, Monte-Carlo simulation (MCS) firstly represents the uncertainties of input random variables (RVs) with a series of samples and then obtains the probability distributions of output RVs through a large number of deterministic power flow (DLF) calculations. The traditional MCS method with simple random sampling (MCS-SRS) [3] usually requires 10^4–10^6 trials to harvest accurate results. The massive computational burden hinders its applications in large-scale power systems. Hence, serval advanced sampling techniques, such as Latin supercube sampling [4], uniform design sampling [5], and Latin hypercube sampling (LHS) [6,7] are introduced to improve the computational efficiency. Besides, combined MCS and parallel computing [8] provides a promising approach for online PLF analysis. It achieves high accuracy at a low computational burden.

As the alternatives for solving PLF, analytical methods can avoid repetitive DLF calculations by linearizing the load flow equations (LFEs). The commonly used approach is the cumulant method, which represents the output cumulants as the linear combination of the input cumulants. Then, serval reconstruction techniques, e.g., expansion series (Gram–Charlier [9], Cornish–Fisher [10], and Edgeworth [11]), Maximum Entropy [12] and Laplace Transform [13] are applied to recover the probability distribution from the obtained output cumulants. Although the cumulant-based method is extensively used to evaluate the impacts of uncertainties, e.g., RES [14] and electric vehicles [15], on power system due to its high computational efficiency, the assumption of linearized LFEs may introduce errors. Moreover, the errors are more notable in the tail regions of the probability distributions. To cope with this issue, [16] develops an analytical method based on holomorphic embedding method, which can maintain the non-linearity of LFEs. This method can significantly improve the accuracy of results, especially in the tail regions. To accurately approximate the multimodal distribution, several promising analytical methods are being developed, including combined cumulant and Gaussian mixture approximation (CCGMA) [2,17], combined cumulant and sequence operation theory [18], and dependent discrete convolution (DDC) [19]. Univariate CCGMA is proposed in Ref. [17] and further developed as Multivariate CCGMA [2]. In these methods, the distributions of output

* Corresponding author.
E-mail address: tangfei@whu.edu.cn (F. Tang).

https://doi.org/10.1016/j.epsr.2019.106193
Received 8 May 2019; Received in revised form 31 December 2019; Accepted 31 December 2019
Available online 10 January 2020
0378-7796/

RVs are expressed as a weighted sum of a series of Gaussian functions. A DDC-based method for PLF analysis is developed in Ref. [19]. This method requires discrete approximation of all continuous distributions. Moreover, a smaller value of input sequence interval is necessary to ensure the high accuracy of results.

Approximation methods are effective in reducing the computational burden while keeping a reasonable accuracy. The mainstream approach is the point estimate method (PEM), which approximates the statistical moments of output RVs using DLF calculation at a few representative points. Based on the number of representative points, PEM can be classified as 2^m, $2m$, and $km + 1$ ($k = 2, 4, 6$) schemes [20], where m is the number of input RVs. In Ref. [21], the performances of ($km + 1$) schemes are evaluated, and the $2m + 1$ scheme gives the best solution in terms of accuracy and computational burden. It is noted that PEM can not directly obtain the probability distributions of outputs. The series expansion techniques are required to approximate the distributions of outputs. Generalized polynomial chaos expansion (gPCE) [22] is an emerging technique, which approximates the output RVs by a series of multivariate orthogonal polynomials. However, when the number of input RVs increases, the efficiency of this method decreases significantly. Some techniques, e.g., least angle regression [23,24] and compressed sensing [25] are introduced to solve the high-dimensional problem.

There has been a significant development for PLF analysis in the last decades. However, three critical challenges still need to be addressed. (1) ***Variability***: the variations of input RVs are abundant, whose probability distributions may be far different from Gaussian distributions. Meanwhile, multimodal distributions of outputs may be introduced in some special cases. (2) ***Correlation***: evidence shows that the dependence exists among input RVs, which makes it necessary to take the correlations into account. Moreover, a comprehensive description of dependence should be included both on the degree and structure. (3) ***Dimensionality***: numerous input RVs in large-scale networks may lead to the problem of the curse-of-dimensionality.

Motivated by the challenges mentioned above, this paper proposes a scenario-based cumulant method (SBCM) for PLF analysis. In this method, the scenario analysis technique [26] is introduced and used to represent the uncertainties of correlated input RVs as the representative scenarios. Then, the cumulant method is applied to obtain the cumulants of outputs with each scenario. Finally, the distributions of outputs are expressed as the weighted sum of a series of Gaussian functions. The appealing advantages of the proposed method are summarized as follows:

- Due to the analytical expression of output RVs, this method has high precision in estimating the multimodal probability distributions and statistical moments of outputs.
- Compared with the existing cumulants-based method, this method can effectively formulate the nonlinear dependencies among various input RVs.
- The computational complexity of this method is related to the number of representative scenarios, and it can effectively avoid curse-of-dimensionality caused by numerous input RVs.

The remainder of this paper is organized as follows. In Section 2, uncertainty modeling is introduced, including modeling of RES generation, load, and their correlations. In Section 3, the stochastic variables processing technique based on scenario analysis is introduced. In Section 4, the proposed SBCM for PLF analysis is explained. In Section 5, the performance of the proposed method is evaluated on the IEEE 14-bus system and 118-bus system. Finally, the conclusion of this work is presented in Section 6.

2. Modeling of uncertainty

The proper modeling of input uncertainties is necessary to achieve an accurate PLF analysis [27]. In this section, the uncertainty of wind power, solar power, and load demand are modeled. Moreover, the Copula theory is applied to characterize the correlation of multiple input RVs.

2.1. Wind generation

It is widely accepted that the wind speed obeys the Weibull distribution [28]. The probability density function (PDF) of Weibull distribution is represented as

$$f(v) = \frac{k}{c}\left(\frac{v}{c}\right)^{k-1}\exp\left(-\left(\frac{v}{c}\right)^{k}\right) \tag{1}$$

where v is the wind speed; k and c are the shape and scale parameters, respectively.

The wind turbine characteristic curve can be expressed by a piecewise function as follows

$$P_{wp}(v) = \begin{cases} 0 & v \le v_{ci} \ \ or \ \ v > v_{co} \\ P_W \dfrac{v - v_{ci}}{v_r - v_{ci}} & v_{ci} \le v \le v_r \\ P_W & v_r < v \le v_{co} \end{cases} \tag{2}$$

where v_{ci}, v_r and v_{co} are the cut-in, rated, and cut-out wind speed, respectively; P_{wp} and P_W are the output and rated power of wind generation, respectively. It is assumed that variable-speed wind generators operate in the constant power factor mode, and reactive power Q_{wp} can be accordingly determined by active power.

2.2. Solar generation

The solar radiation can be described by Beta distribution [29]:

$$f(r) = \frac{\Gamma(\alpha+\beta)}{\Gamma(\alpha)\Gamma(\beta)}\left(\frac{r}{r_{\max}}\right)^{\alpha-1}\left(1 - \frac{r}{r_{\max}}\right)^{\beta-1} \tag{3}$$

where r and $r_{\max}$ are the actual and maximum solar radiations, respectively; α and β are parameters of this distribution; $\Gamma(\cdot)$ is the Gamma function.

The relationship between solar radiation and output power is expressed as follows:

$$P_{pv}(r) = \begin{cases} P_S \dfrac{r^2}{r_c r_{std}} & r < r_c \\ P_S \dfrac{r}{r_{std}} & r_c \le r \le r_{std} \\ P_S & r > r_{std} \end{cases} \tag{4}$$

where r_c is a certain radiation point; r_{std} is the solar radiation in the standard environment; P_{pv} and P_S are the output power and rated power of the photovoltaic unit, respectively. Solar generation is usually required to operate in the unity power factor mode. Hence the reactive power is set to zero.

2.3. Load variation

In general, the uncertainty of load consumption is described by Gaussian distribution. The expected value is the base load power, and the standard deviation is 5%–10% of the expected value. In some special cases, the load consumption can also be modeled by a discrete distribution with finite values [17].

2.4. Correlation of input variables

According to the Sklar's theorem [30], the joint cumulative distribution function (CDF) of an m-dimensional input variable $\boldsymbol{w} = [w_1, ..., w_l, ..., w_m]^{\mathrm{T}}$ can be represented by the univariate CDFs and a Copula function that characterizes their dependences. Therefore, the joint CDF of $\boldsymbol{w}$ can be expressed as

$$F_{\boldsymbol{w}}(\boldsymbol{w}) = C(F_{w_1}(w_1),\ ...,F_{w_l}(w_l),\ ...,F_{w_m}(w_m)) \tag{5}$$

where $F_{w_l}(w_l)$ is the marginal distribution of w_l; $C(\cdot)$ is the Copula function.

Various Copula functions have been proposed in the literature, and the typical Copula functions include Gaussian copula, Student-t copula, Clayton copula and so on. Different Copula functions are suitable to characterize different dependence structures, and the selection of optimal Copula function can be based on the goodness of fit [31]. Since the selection of suitable Copula function is out of the purpose of this paper, the Gaussian Copula which is more flexible for multivariate correlation modeling is used in this work.

The correlation of Gaussian Copula function can be parameterized by Kendall's rank correlation coefficient [19]. Hence, the multivariate correlation can be described using Kendall's rank correlation coefficient matrix C_D as follows

$$C_D = \begin{bmatrix} C_{RES} & C_{RES-Load} \\ C_{RES-Load}^{\mathrm{T}} & C_{Load} \end{bmatrix} \tag{6}$$

where C_{RES}, C_{Load} and $C_{RES-Load}$ respectively denote Kendall's rank correlation coefficients among RES outputs, loads and the correlations between them.

3. Scenario analysis of stochastic variable

Scenario analysis is a useful tool to solve stochastic problems, which has been widely applied in economic dispatch problems [26] and planning [32] of power systems with renewable energy. In this section, the uncertainties and correlations of input RVs are reproduced by the scenario analysis technique. Moreover, the benefits of this technique for the PLF problem will be discussed in detail in Section 4.2.

3.1. Scenarios generation

Scenario generation is the process of representing uncertainty with a number of certain scenarios. Sampling techniques are commonly used to generate scenarios based on the distributions and correlations of uncertainty factors. In this paper, the efficient stratified sampling technique, i.e., LHS [31], is used to generate original scenarios.

Consider an m-dimensional random vector $\boldsymbol{w} = [w_1,...,w_l,...,w_m]^{\mathrm{T}}$, and the joint distributions of it can be expressed as (5). Let $u_l = F_{w_l}(w_l)$ and $u_l \sim U(0, 1)$, then (5) is transformed as $F(\boldsymbol{u}) = C(u_1,\ ...,u_l,\ ...,u_m)$. The procedure of scenario generation consists of two major steps. Firstly, generate sample matrix $\boldsymbol{U}_{m\times N} = [\boldsymbol{u}_1,...,\boldsymbol{u}_l,...,\boldsymbol{u}_m]^{\mathrm{T}}$ ($\boldsymbol{u}_l = [u_{l1},\ ...,u_{li},\ ...u_{lN}]^{\mathrm{T}}$) by the LHS technique according to the joint distribution $F(\boldsymbol{u})$. Then, transform the sample matrix $\boldsymbol{U}_{m\times N}$ to $\boldsymbol{W}_{m\times N}$ using the inverse function $\boldsymbol{w} = F_{\boldsymbol{w}}^{-1}(\boldsymbol{u})$.

The sample matrix is shown in Fig. 1. $\boldsymbol{W}_{m\times N} = [\boldsymbol{w}_1,...,\boldsymbol{w}_l,...,\boldsymbol{w}_m]^{\mathrm{T}}$ is defined as the original scenario set, and each column of it, i.e., $\omega_i = [w_{1i},...w_{li},...,w_{mi}]^{\mathrm{T}}$, is defined as a scenario.

3.2. Scenarios reduction

A larger number of scenarios might have higher accuracy for describing the uncertainties. However, numerous scenarios would lead to redundancy with a higher computational burden. To reduce the computational burden and maintain a certain accuracy, a scenario reduction technique named simultaneous backward reduction (SBR) [33] is applied to obtain the representative snapshots of input RVs.

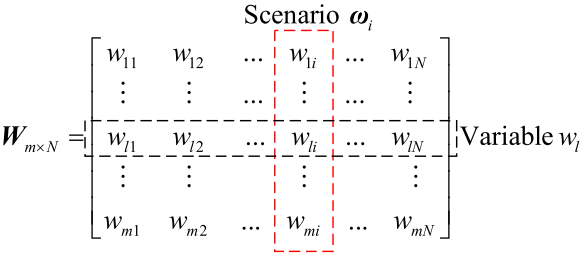

Fig. 1. Original scenarios of $\boldsymbol{w}$.

Assume the original set has N scenarios $\omega = \{\omega_1,...,\omega_i,\ ..,\ \omega_N\}$, where $\omega_i = [w_{1i},...w_{li},...,w_{mi}]^{\mathrm{T}}$. Denote N_s is the number of representative scenarios after reduction. The probability of each scenario ω_i is equally set as $\pi^{(\omega_i)} = 1/N$. The number of remaining scenarios in the process of scenario reduction is set as n_s. The procedure of the SBR algorithm can be expressed as the following:

i. Calculate the Kantorovich distance between ω_i and ω_j as follows

$$d(\omega_i,\ \omega_j) = \sqrt{\sum_{l=1}^{m}(w_{li} - w_{lj})} \tag{7}$$

ii. Determine the non-representative scenario ω_s which meets the requirement of (8)

$$P_{\mathrm{KD}s} = \min\{P_{\mathrm{KD}i} | 1 \le i \le n_s\} \tag{8}$$

where $P_{\mathrm{KD}i} = \min\{d(\omega_i,\ \omega_j) | i \ne j\} \times \pi^{(\omega_i)}$;

iii. Eliminate the non-representative scenario ω_s, and change the total number of remaining scenarios, i.e., $n_s = n_s - 1$;

iv. Pick out the scenario ω_i^* nearest to the eliminated scenario ω_s, and redistribute the probability of ω_i^* as follows

$$\pi^{(\omega_i^*)} = \pi^{(\omega_i^*)} + \pi^{(\omega_s)} \tag{9}$$

v. Repeat the SBR algorithm Steps ii.–iv. until the total number of remaining scenarios n_s equals N_s.

Through the procedure of scenario generation and reduction in 3.1 and 3.2, the uncertainties of correlated input RVs can be expressed as a small number of representative scenarios.

4. Scenario-based cumulant method for PLF

In this section, the theoretical background of the cumulant method is present. After that, the proposed method for PLF analysis is explained. Finally, the computational procedure of the method is summarized.

4.1. Cumulant method

The nonlinear power flow equations can be expressed as follows:

$$\begin{cases} \boldsymbol{W} = \boldsymbol{f}(\boldsymbol{X}) \\ \boldsymbol{Z} = \boldsymbol{g}(\boldsymbol{X}) \end{cases} \tag{10}$$

where $\boldsymbol{W}$ is the vector of power injections; $\boldsymbol{X}$ is the vector of bus voltages (magnitudes and angles); $\boldsymbol{Z}$ is the vector of branch power flows (active and reactive power), respectively; $\boldsymbol{f}(\cdot)$ and $\boldsymbol{g}(\cdot)$ are the nodal power and line flow functions, respectively.

Eq. (10) can be linearized at the point of the expected operation status:

$$\begin{cases} \boldsymbol{W} = \boldsymbol{f}(\boldsymbol{X}) = \boldsymbol{W}_0 + \Delta\boldsymbol{W} \\ = \boldsymbol{f}(\boldsymbol{X}_0 + \Delta\boldsymbol{X}) \approx \boldsymbol{f}(\boldsymbol{X}_0) + \boldsymbol{J}_0\Delta\boldsymbol{X} \\ \boldsymbol{Z} = \boldsymbol{g}(\boldsymbol{X}) = \boldsymbol{Z}_0 + \Delta\boldsymbol{Z} \\ = \boldsymbol{g}(\boldsymbol{X}_0 + \Delta\boldsymbol{X}) \approx \boldsymbol{g}(\boldsymbol{X}_0) + \boldsymbol{G}_0\Delta\boldsymbol{X} \end{cases} \tag{11}$$

where $\Delta\boldsymbol{W}$ represents the variations of power injections; $\Delta\boldsymbol{X}$ and $\Delta\boldsymbol{Z}$ are the variations of bus voltages and branch power flows, respectively; $\boldsymbol{J}_0$ and $\boldsymbol{G}_0$ can be calculated by partial derivatives

$$\begin{cases} \boldsymbol{J}_0 = (\partial\boldsymbol{W}/\partial\boldsymbol{X})|_{\mathbf{X}=\mathbf{X_0}} \\ \boldsymbol{G}_0 = (\partial\boldsymbol{Z}/\partial\boldsymbol{X})|_{\boldsymbol{X}=\boldsymbol{X_0}} \end{cases} \tag{12}$$

Based on Eq. (11), the relationship among bus voltages, branch power flows and injected powers at the reference point can be

expressed as follows

$$\begin{cases}\Delta \boldsymbol{X} = \boldsymbol{J}_0^{-1}\Delta \boldsymbol{W} = \boldsymbol{S}_0\Delta \boldsymbol{W} \\ \Delta \boldsymbol{Z} = \boldsymbol{G}_0\boldsymbol{J}_0^{-1}\Delta \boldsymbol{W} = \boldsymbol{T}_0\Delta \boldsymbol{W}\end{cases} \tag{13}$$

where $\boldsymbol{S}_0 = \boldsymbol{J}_0^{-1}$ and $\boldsymbol{T}_0 = \boldsymbol{G}_0\boldsymbol{J}_0^{-1}$.

Eq. (13) indicates the linear relationships between the input and output RVs. Hence, based on the properties of cumulants, the cumulants of desired outputs can be represented as the linear combinations of the cumulants of inputs [11].

$$\begin{cases}\gamma_{\boldsymbol{X}} = \boldsymbol{S}_0\gamma_{\boldsymbol{W}} \\ \gamma_{\boldsymbol{Z}} = \boldsymbol{T}_0\gamma_{\boldsymbol{W}}\end{cases} \tag{14}$$

where $\gamma_{\boldsymbol{W}}$, $\gamma_{\boldsymbol{X}}$, and $\gamma_{\boldsymbol{Z}}$ are the cumulants of injected power, bus voltages, and branch power flows, respectively.

It is noticeable that if the input RVs $\Delta \boldsymbol{W}$ are independent, the cumulants of output RVs can be directly calculated by Eq. (14). Otherwise, the joint cumulants of correlated input RVs should be considered [11]. However, due to the implementation of long expansions of joint cumulants, the cumulant method cannot effectively deal with the nonlinear correlations among input RVs [34].

4.2. Scenario-based cumulant method

In the context of power grids, the uncertainties mainly come from RES output and load demand. The uncertain of RES generation is commonly modeled by a non-Gaussian distribution, while the load demand is assumed to obey the Gaussian distribution.

The uncertainties of non-Gaussian RES generations can be expressed as the representative scenarios, i.e., $\omega^* = \{\omega_1^*, ...,\omega_i^*, ...,\omega_{N_S}^*\}$ through the scenario analysis technique in Section 3. For each scenario ω_i^*, the injected powers of RES are constant values. Meanwhile, the variations of load demands follow Gaussian distributions. Under these conditions, the cumulant method (11)–(14) is used to calculate the cumulants of output RVs. It can be seen from the linear relation in Eq. (13) that the output RVs also obeys the Gaussian distribution. Since the first two order cumulants, i.e., expected value and standard deviation are adequate to represent Gaussian distribution. The PDFs and CDFs of output RVs with the scenario ω_i^* can be expressed as follows:

$$f(\boldsymbol{x}|\omega_i^*) = \frac{1}{\sqrt{2\pi\boldsymbol{\sigma}_i^2}}\exp\left(\frac{-(\boldsymbol{x}-\boldsymbol{\mu}_i)^2}{2\boldsymbol{\sigma}_i^2}\right) \tag{15}$$

$$F(\boldsymbol{x}|\boldsymbol{\omega}_{\boldsymbol{i}}^*) = \int_{-\infty}^{\boldsymbol{x}}\frac{1}{\sqrt{2\pi\boldsymbol{\sigma}_i^2}}\exp\left(\frac{-(\xi-\boldsymbol{\mu}_i)^2}{2\boldsymbol{\sigma}_i^2}\right)d\xi \tag{16}$$

where $\boldsymbol{x}$ is the vector of output RVs; $\boldsymbol{\mu}_i$ and $\boldsymbol{\sigma}_i$ are the vectors of expected values and standard deviations of $\boldsymbol{x}$ with scenario ω_i^*, respectively.

Execute the cumulant method with each scenario in vector ω^*. Then, based on *the Law of Total Probability* [35], the entire probabilistic distribution of output RVs can be obtained by integrating the distributions and the corresponding weight of each scenario. The final results are expressed as

$$\begin{aligned}f(\boldsymbol{x}|\boldsymbol{\omega}^*) &= \pi^{(\omega_1^*)}\cdot f(\boldsymbol{x}|\boldsymbol{\omega}_{\boldsymbol{1}}^*)+...+\pi^{(\omega_{N_S}^*)}\cdot f(\boldsymbol{x}|\boldsymbol{\omega}_{N_S}^*) \\ &= \sum_{i=1}^{N_S}\left(\pi^{(\omega_i^*)}\frac{1}{\sqrt{2\pi\boldsymbol{\sigma}_i^2}}\exp\left(\frac{-(\boldsymbol{x}-\boldsymbol{\mu}_i)^2}{2\boldsymbol{\sigma}_i^2}\right)\right)\end{aligned} \tag{17}$$

$$\begin{aligned}F(\boldsymbol{x}|\boldsymbol{\omega}^*) &= \pi^{(\omega_1^*)}\cdot F(\boldsymbol{x}|\boldsymbol{\omega}_1^*)+...+\pi^{(\omega_{N_S}^*)}\cdot F(\boldsymbol{x}|\boldsymbol{\omega}_{N_S}^*) \\ &= \sum_{i=1}^{N_S}\left(\pi^{(\omega_i^*)}\int_{-\infty}^{\boldsymbol{x}}\frac{1}{\sqrt{2\pi\boldsymbol{\sigma}_i^2}}\exp\left(\frac{-(\boldsymbol{\xi}-\boldsymbol{\mu}_i)^2}{2\boldsymbol{\sigma}_i^2}\right)d\boldsymbol{\xi}\right)\end{aligned} \tag{18}$$

where $\pi^{(\omega_i^*)}$ is the occurrence probability of scenario ω_i^*.

It can be seen from Eqs. (17) and (18) that the probability distributions of outputs are analytically expressed as the weighted sum of a series of Gaussian functions. Therefore, the probability distribution of the outputs can be obtained by the samples of these Gaussian distributions.

In addition to the probability distribution, the statistical moments of variables are also essential to characterize the uncertainties, especially, the expected values and standard deviations. In this method, the statistical moments of outputs can be obtained through their cumulants.

Let x be the desired output, the r-th ($r = 1, 2$) raw moment of it can be obtained as follows

$$\alpha_x^r = \pi^{(\omega_1^*)}\cdot\alpha_{x1}^r + ...+\pi^{(\omega_{N_S}^*)}\cdot\alpha_{xN_S}^r = \sum_{i=1}^{N_S}\left(\pi^{(\omega_i^*)}\cdot\alpha_{xi}^r\right) \tag{19}$$

where α_{xi}^r is the raw moment of x with the scenario ω_i^*.

According to the relationship between the moments and cumulants [36], the first two order moments of x with scenario ω_i^* can be obtained by its cumulants

$$\begin{cases}\alpha_{xi}^1 = \gamma_{xi}^1 \\ \alpha_{xi}^2 = \gamma_{xi}^2 + \left(\gamma_{xi}^1\right)^2\end{cases} \tag{20}$$

where γ_{xi}^1 and γ_{xi}^2 are the first two order cumulants of x in scenario ω_i^*, respectively.

Combine (19) and (20) to calculate the r-th ($r = 1, 2$) order moment α_x^r, then the expected value and standard deviation of x can be calculated as follows:

$$\begin{cases}\mu_x = \alpha_x^1 \\ \sigma_x = \sqrt{(\alpha_x^2 - (\alpha_x^1)^2)}\end{cases} \tag{21}$$

where α_x^1 and α_x^2 are the first two order moments of x, respectively.

In the above description of the proposed method, the uncertainties from renewable generations and load fluctuations are considered. Moreover, the proposed method can also be expanded to consider more types of input uncertainties, such as unavailability of the generation unit [1], which is represented by binomial distributions. As shown in Fig. 2, the input uncertainties can be modeled by non-Gaussian or Gaussian distributions. The proposed method uses multiple representative scenarios to represent the uncertainties following non-Gaussian distributions. The remaining uncertainties follow Gaussian distributions. Then, the cumulant method is performed on each scenario to obtain the probability distributions of outputs, as shown in Eq. (15). The entire distributions of outputs can be calculated using Eqs. (17) and (18). Thanks to the scenarios-based technique, the proposed method can deal with various types of non-Gaussian uncertainties.

The advantages of the proposed method are explained as follows: Firstly, the analytical expressions in Eqs. (17) and (18) can guarantee high accuracy in approximating the distributions of output RVs, which has been proved in literature [2,17]. Secondly, since the correlated RES outputs which follow non-Gaussian are expressed as the representative scenarios, the injected powers of RES in each scenario are constant values. That means the joint cumulants of RES outputs can be avoided when performing the cumulant method. This simplification makes the proposed method more efficient in considering correlations among the RES outputs, especially the nonlinear correlation. Finally, the computational complexity of this method is linearly related to the number of representative scenarios, rather than the number of input RVs. Thus the "curse-of-dimensionality" can be effectively avoided.

4.3. Computational procedure of SBCM

The computational procedure of the proposed SBCM is shown in Fig. 3, whose major steps are summarized as follows:

Step 1: Read the necessary data for PLF, such as network topologies, load demands, parameters of RES, and Kendall's rank correlation coefficient matrix;

Step 2: Establish the original scenarios $\omega = \{\omega_1, ..., \omega_i, ..., \omega_N\}$ for non-

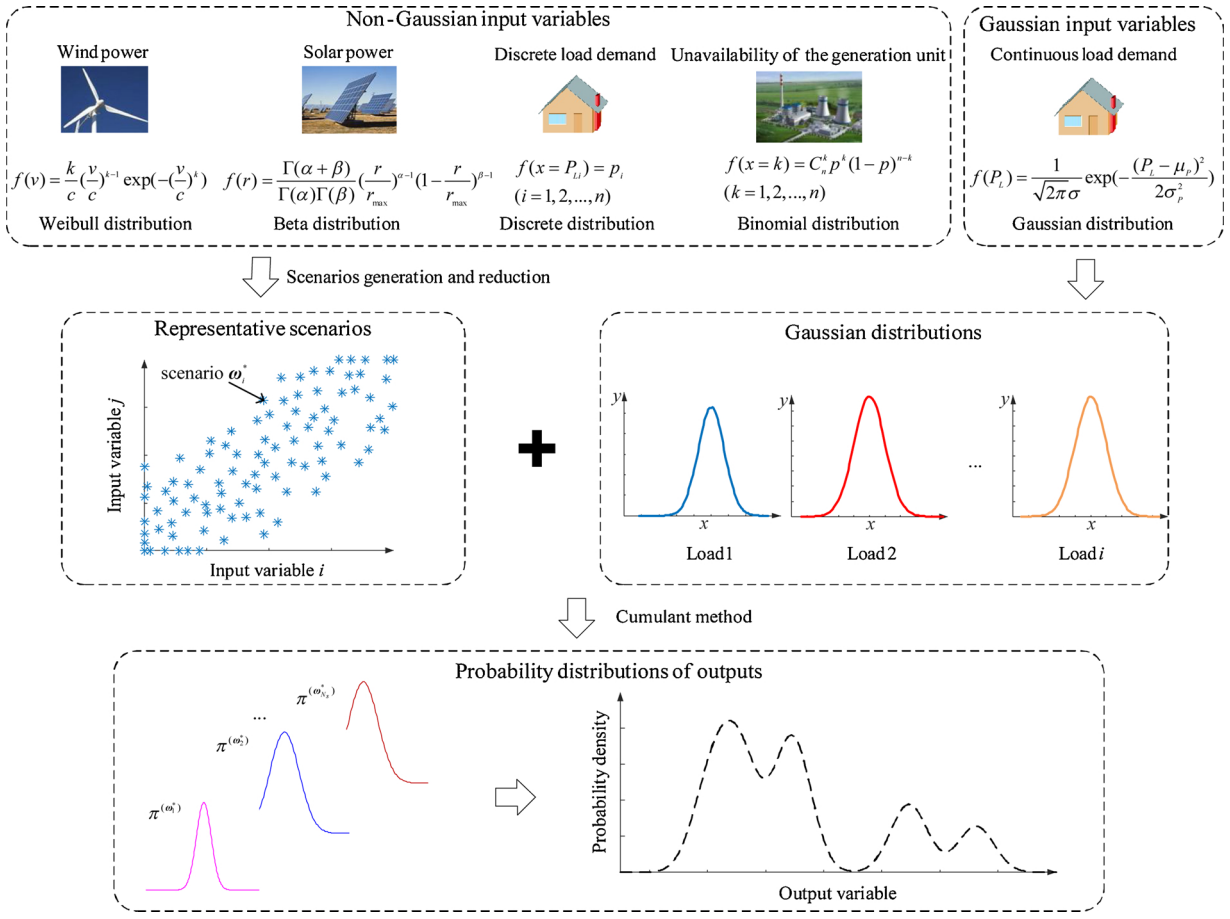

Fig. 2. The description of the proposed SBCM.

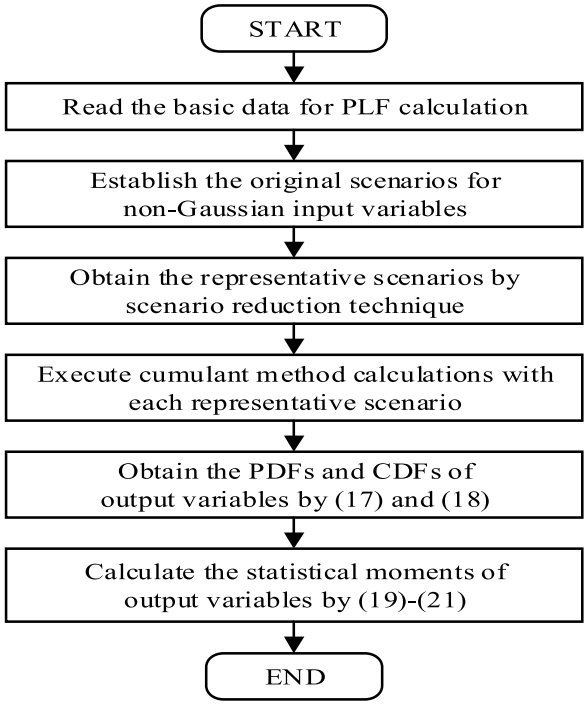

Fig. 3. The procedure of SBCM for PLF analysis.

Gaussian input RVs according to the procedure in Section 3.1;

Step 3: Perform the scenario reduction technique to obtain a reduced number of representative scenarios $\omega^* = \{\omega_1^*, ..., \omega_i^*, ..., \omega_{N_s}^*\}$;

Step 4: Execute the cumulant method with each representative scenario ω_i^* to obtain the corresponding expected values and standard deviations of output RVs;

Step 5: Reconstruct the PDFs and CDFs of output RVs by the weighted sum of a series of Gaussian functions based on Eqs. (17) and (18);

Step 6: Obtain the statistical moments of desired output RVs by Eqs. (19) and (21).

5. Case study

In this section, the performance of SBCM is evaluated on the IEEE 14-bus system and 118-bus system. Uncertainties caused by load demands and RES as well as their correlations are considered. The results obtained by MCS-SRS are used as the comparative reference, and the sample size of MCS is determined by the coefficient of variation [2], i.e., $\beta_{\max} < 1\%$ for all outputs. The numerical experiments are implemented in MATPOWER toolbox [37] on a PC with Intel Core i7 2.5 GHz and 8GB of RAM.

5.1. Convergence check

The relative error in Eq. (22) and average root mean square (ARMS) error in Eq. (23) [13] are applied to evaluate the accuracy of SBCM:

$$\varepsilon_s^\gamma = \left| \frac{m_s^\gamma - m_{s,\mathrm{MCS}}^\gamma}{m_{s,\mathrm{MCS}}^\gamma} \right| \times 100\% \tag{22}$$

$$\mathrm{ARMS}^{\gamma} = \frac{1}{n}\sqrt{\sum_{i=1}^{N}\left(M_i^{\gamma} - C_i^{\gamma}\right)} \times 100\% \tag{23}$$

where γ represents the type of output RVs; the subscript s denotes the statistical characteristics of variable, e.g., mean value μ and standard deviation σ; $m_{s,\mathrm{MCS}}^{\gamma}$ and m_s^{γ} are the statistical results obtained by MCS-SRS and the method to be evaluated, respectively. M_i^{γ} and C_i^{γ} are the i-th evaluation point's value on the CDF curves obtained by MCS-SRS and the method to be evaluated, respectively; n in the denominator of (23) is the number of evaluation points, and $n = 200$ is assumed in this study.

The mean value and max value of the relative error, i.e., $\varepsilon_{s,mean}^{\gamma}$ and $\varepsilon_{s,\max}^{\gamma}$, are used to indicate the accuracy and robustness of the proposed method. Additionally, due to the random sampling technique used in forming the representative scenarios, the proposed method with a specific number of scenarios will run 100 times independently to obtain an accurate evaluation. The average values of these 100 trials, i.e., $\bar{\varepsilon}_{s,mean}^{\gamma}$ and $\bar{\varepsilon}_{s,\max}^{\gamma}$, are adopted as the final error indexes.

5.2. IEEE 14-bus system

In the study case on the IEEE 14-bus system, two solar parks are installed at Bus 13 and 14. The solar radiation and technical parameters of the solar parks are shown in Table 1. The loads at all buses except Bus 9 obey Gaussian distribution. Suppose the expected value is the base load power, and the standard deviation is 10% of the expected value. The load at Bus 9 follow the discrete distribution, and the parameters are given in Table 2. The correlations among solar parks and adjacent loads are considered with their Kendall's rank correlation coefficient matrix given in Table 3.

Firstly, generate the representative scenarios of non-Gaussian stochastic variables based on the scenario analysis technique. There are 1000 original scenarios, i.e., $N = 1000$. Eight different sizes of representative scenarios, i.e., $N_s = 100$–800, are compared to demonstrate the impact of scenarios number on PLF results. The errors of branch active power $\boldsymbol{P}$ are selected to demonstrate this impact.

The error results of branch active power with different N_s are shown in Fig. 4, from which the impact of N_s on the performance of the proposed method is illustrated. On the one hand, the increase of N_s improves the accuracy of the method. It is because the increasing of N_s can better represent the uncertainties of input RVs. On the other hand, the improvement of accuracy can be negligible, when the number of representative scenarios exceeds 300, over which the results converge. Therefore, 300 representative scenarios are adequate to obtain accurate PLF results in this case study.

In order to show the superiority of the proposed SBCM, the well-established MCS-LHS with 1000 trails is implemented to render comparative results. The comparisons of relative errors are shown in Table 4. The largest errors of mean values and standard deviations obtained by the proposed method are less than 1% and 2%, respectively. The small values of errors indicate that the method can obtain accurate estimations in statistical moments for different types of output RVs. Compared with the MCS-LHS, the proposed SBCM can achieve higher accuracy in the estimation of the standard deviations with fewer trials of calculations.

The graphical results of the output RVs are also presented to

Table 2
Parameters of discrete load power at Bus 9 [17].

Load Power	Capacity (p.u.)				
P_{load9}	0.134	0.196	0.302	0.348	0.373
Q_{load9}	0.075	0.110	0.170	0.196	0.210
Probability value	0.100	0.150	0.300	0.250	0.200

Table 3
Kendall's rank correlation coefficient matrix.

Random Variable	P_{pv13}	P_{pv14}	P_{load13}	P_{load13}	Q_{load13}	Q_{load14}
P_{pv13}	1	0.41	0.19	0.13	0	0
P_{pv14}	0.41	1	0.13	0.19	0	0
P_{load13}	0.19	0.13	1	0.33	0.33	0.13
P_{load14}	0.13	0.19	0.33	1	0.13	0.33
Q_{load13}	0	0	0.33	0.13	1	0.33
Q_{load14}	0	0	0.13	0.33	0.33	1

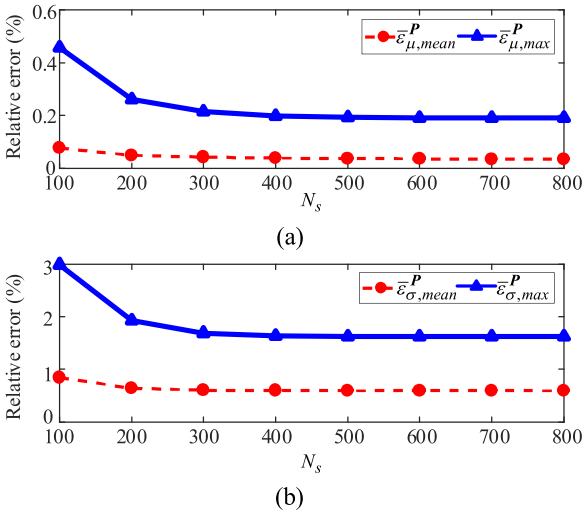

Fig. 4. Relative error $\bar{\varepsilon}_{\mu}^{\boldsymbol{P}}$ (a) and $\bar{\varepsilon}_{\sigma}^{\boldsymbol{P}}$ (b) of branch active power with different scenarios number.

Table 4
Relative error comparisons of two methods.

Relative error (%)	SBCM (N_s = 300)		MCS-LHS (1000 trials)	
	Mean	Max	Mean	Max
$\bar{\varepsilon}_{\mu}^{\boldsymbol{V}}$	0.0016	0.0027	0.0005	0.0013
$\bar{\varepsilon}_{\sigma}^{\boldsymbol{V}}$	0.470	1.182	0.862	2.296
$\bar{\varepsilon}_{\mu}^{\boldsymbol{\theta}}$	0.026	0.041	0.007	0.010
$\bar{\varepsilon}_{\sigma}^{\boldsymbol{\theta}}$	0.702	1.083	1.335	1.951
$\bar{\varepsilon}_{\mu}^{\boldsymbol{P}}$	0.043	0.216	0.029	0.184
$\bar{\varepsilon}_{\sigma}^{\boldsymbol{P}}$	0.606	1.691	1.171	3.045
$\bar{\varepsilon}_{\mu}^{\boldsymbol{Q}}$	0.309	1.294	0.071	0.542
$\bar{\varepsilon}_{\sigma}^{\boldsymbol{Q}}$	0.744	1.863	0.978	3.068

Table 1
Solar radiation and solar park parameters.

Bus	α [kW/m^2]	β [kW/m^2]	$r_{\min}$ [W/m^2]	$r_{\max}$ [W/m^2]	R_c [W/m^2]	R_{std} [W/m^2]	P_S [MW]
13	2.5	4.2	0	1000	150	1000	10
14	3	4	0	1000	150	1000	10

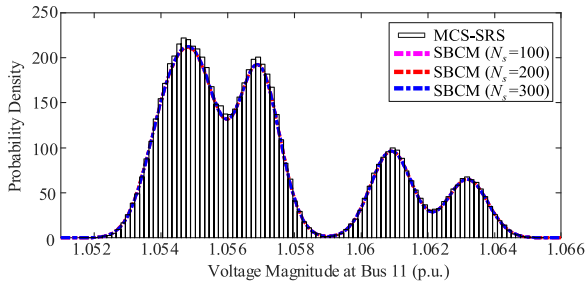

Fig. 5. Probability density curves of voltage magnitude at Bus 11.

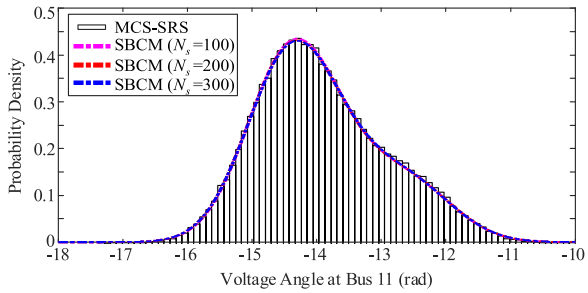

Fig. 6. Probability density curves of voltage angle at Bus 11.

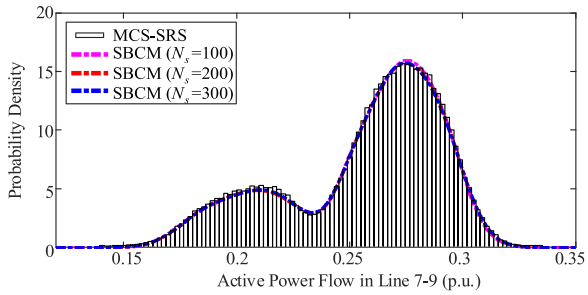

Fig. 7. Probability density curves of active power flow in line 7–9.

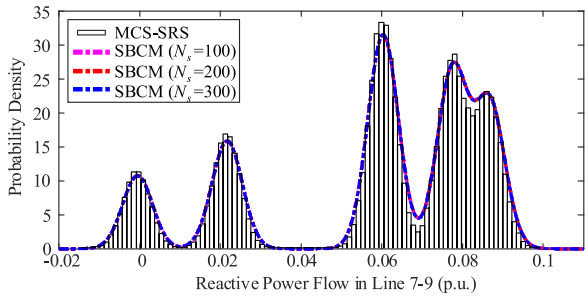

Fig. 8. Probability density curves of reactive power flow in line 7–9.

Table 5
ARMS error of output variables.

Random Variable	ARMS (%)		
	N_s = 100	N_s = 200	N_s = 300
V_{11}	0.0168	0.0168	0.0168
θ_{11}	0.0183	0.0168	0.0168
P_{7-9}	0.0348	0.0341	0.0341
Q_{7-9}	0.0213	0.0211	0.0211

demonstrate the effectiveness of SBCM. The probability distributions obtained by SBCM with 100, 200 and 300 scenarios are shown in Figs. 5–8. The results obtained by MCS-SRS are used as a reference. As it is observed from the figures, the probability distributions of V_{11}, $P_{7\text{-}9}$, and $Q_{7\text{-}9}$ follow multimodal distributions, while the probability distribution of θ_{11} is also far different from the Gaussian distribution. In these figures, the empirical results obtained by MCS-SRS can be well approximated by the proposed SBCM. Meanwhile, the results obtained by SBCM with different N_s have minor differences from each other. The ARMS error is adopted to analyze the accuracy of the probability distribution quantitatively, and the results are shown in Table 5. The results indicate that the method can achieve high accuracy with only 100 representative scenarios.

As an essential application of PLF, the risk assessment of events, e.g., bus under/overvoltage and line flow overload, is of great interest for power system operators. The accuracy of risk assessment depends on the reliable tail regions of distribution [27,39]. In order to verify the performance of the proposed method in estimating risk events, the Cross-Entropy-based MCS (MCS-CE) is performed as a comparison. MCS-CE method shows excellent performance in the reliability evaluation [38] and risk assessment [39] of power systems. In this method, the distributions of inputs are duly distorted, so that the important regions are sampled more often, thus accelerating the convergence rate of MCS. The stopping criterion of MCS is set as $\beta < 1\%$. The required sample sizes and computation time of MCS-SRS and MCS-CE are shown in Table 6. The results of risk events are presented in Table 7.

It is evident that the probabilities of risk events are very small, and MCS-SRS requires a large number of samples to reach the stopping criterion. By contrast, MCS-CE can yield accurate results, significantly reducing the sample size and improving efficiency by at least 22 times. Compared with MCS-SRS and MCS-CE, the proposed method takes fewer load flow calculations to obtain the risk results with reasonable accuracy. Therefore, it has the advantage of high efficiency. The proposed method can help operators quickly and accurately identify the variables that may endanger the system and provide target variables for further high-precision analysis.

Besides the accuracy analysis, the computational burden is another criterion, which is composed of four parts:

$$T_{TOTAL} = T_{SG} + T_{SD} + T_{CM} + T_{POST} \tag{24}$$

where T_{SG} is the time consumed to generate the initial scenarios; T_{SD} is the time to form the representative scenarios; T_{CM} is the time to perform the cumulant method with each representative scenario; T_{POST} is the time used in formulating the probability distributions based on the obtained mean values and standard deviations.

Let voltage magnitude V_{11} be the desired output response, 5000 samples are involved in reconstructing its probability distribution. The required computation time of SBCM with 100, 300, and 500 scenarios are listed in Table 8. The computational burdens of MCS-SRS and MCS-LHS are set as the reference.

The results show that MCS-SRS requires 58.05 s to reach the preset stopping criterion. In contrast, MCS-LHS can significantly reduce the computation burden of MCS-SRS Due to the advanced sampling techniques. The computational burdens of SBCM are shown in Row 3–5 of Table 8. The proposed method can dramatically alleviate the computational burden of the MCS-SRS and achieve at least 10 (58.05/4.93) times speed-up on efficiency. The total computation time of SBCM increases with the larger scenario size, which mainly due to the increase

Table 6
Performance of MCS-SRS and MCS-CE for risk assessment.

Risk events	Samples		Time (s)	
	MCS-SRS	MCS-CE	MCS-SRS	MCS-CE
$V_{11} > 1.064$ p.u.	1010000	31000	2602	115
$V_{11} < 1.053$ p.u.	1234000	37000	3500	131
$P_{7\text{-}9} > 0.315$ p.u.	4712000	103000	11945	305
$P_{7\text{-}9} < 0.165$ p.u.	4315000	79000	10935	265

Table 7
Probability of violation of output variables.

Probability ($\times 10^{-3}$)	SBCM (N_s = 100)	SBCM (N_s = 200)	SBCM (N_s = 300)	MCS-SRS	MCS-CE
$Pr(V_{11} > 1.064$ p.u.)	9.493	9.537	9.545	9.677	9.731
$Pr(V_{11} < 1.053$ p.u.)	7.098	7.156	7.177	7.324	7.272
$Pr(P_{7\text{-}9} > 0.315$ p.u.)	1.989	2.021	2.075	2.117	2.146
$Pr(P_{7\text{-}9} < 0.165$ p.u.)	2.233	2.302	2.311	2.315	2.283

Table 8
Computational burden analysis of IEEE 14-bus test system (s).

Method	T_{TOTAL}	T_{SG}	T_{SD}	T_{CM}	T_{POST}
MCS-SRS	58.05	–	–	–	–
MCS-LHS (1000 trials)	5.27	–	–	–	–
SBCM (N_s = 100)	3.32	0.06	2.68	0.56	0.02
SBCM (N_s = 300)	3.94	0.06	2.38	1.57	0.03
SBCM (N_s = 500)	4.93	0.06	2.16	2.66	0.05

of T_{CM}. According to the accuracy analysis, the redundancy of scenarios only adds unimportant details but at the expense of much heavier computational burden. Therefore, an appropriate number of representative scenarios may achieve a compromise between accuracy and efficiency.

5.3. IEEE 118-bus system

The IEEE 118-bus system is also applied to test the performance of SBCM. All loads are represented by the Gaussian distribution, whose standard deviations are 10% of their expected values. Eight wind farms and four solar parks are integrated into the systems. The technical parameters of wind farms and solar parks are shown in Tables 9 and 10, respectively.

Wind farms are classified into two groups. The wind power outputs in the same group are assumed to be correlated, while the wind power outputs in the different groups are considered independent. The outputs of solar parks are also correlated. The correlation coefficient matrixes are given as below:

$$C_{WP\text{-Group1}} = \begin{bmatrix} 1 & 0.57 & 0.56 & 0.50 \\ 0.57 & 1 & 0.54 & 0.51 \\ 0.56 & 0.54 & 1 & 0.60 \\ 0.50 & 0.51 & 0.60 & 1 \end{bmatrix}$$

$$C_{WP\text{-Group2}} = \begin{bmatrix} 1 & 0.51 & 0.45 & 0.41 \\ 0.51 & 1 & 0.45 & 0.48 \\ 0.45 & 0.45 & 1 & 0.40 \\ 0.41 & 0.48 & 0.40 & 1 \end{bmatrix}$$

$$C_{PV} = \begin{bmatrix} 1 & 0.54 & 0.46 & 0.36 \\ 0.54 & 1 & 0.48 & 0.44 \\ 0.46 & 0.48 & 1 & 0.45 \\ 0.36 & 0.44 & 0.45 & 1 \end{bmatrix}$$

The number of original scenarios N = 1000. The proposed SBCM is conducted with five different numbers of representative scenarios, i.e., N_s = 100–500. The relative errors are shown in Table 11. The results indicate that the method can achieve high accuracy in a larger scale power system. Meanwhile, the accuracy of SBCM is higher with more representative scenarios, but the improvement is negligible when the number of scenarios exceeds 300.

The probability density curves of V_{30} and $P_{6\text{-}7}$ are shown in Figs. 9 and 10, respectively. In these figures, the output RVs follow multimodal distribution due to the significant uncertainties of RES. Although some accuracy of SBCM is lost when the number of representative scenarios N_s = 100, the shape of distributions remains similar, and with the increasing of N_s, the proposed method can achieve high accuracy in approximating multimodal distributions.

Table 9
Wind speed and wind farms parameters.

Bus	Group	v_{ci} [m/s]	v_r [m/s]	v_{co} [m/s]	c	k	P_W [MW]
6/12/15/27	1	3	12	25	8	1.4	80
76/80/100/116	2	3	12	25	7.2	2.2	80

Table 10
Solar radiation and solar parks parameters.

Bus	α [kW/m^2]	β [kW/m^2]	$r_{\min}$ [W/m^2]	$r_{\max}$ [W/m^2]	R_c [W/m^2]	R_{std} [W/m^2]	P_S [MW]
30/40	2.4	4.3	0	1000	150	1000	50
50/60	3.2	3.9	0	1000	150	1000	50

Table 11
Relative errors of output variables (%).

Relative error (%)	SBCM (N_s = 100)	SBCM (N_s = 200)	SBCM (N_s = 300)	SBCM (N_s = 400)	SBCM (N_s = 500)
$\bar{\varepsilon}^{V}_{\mu,mean}$	0.0015	0.0012	0.0012	0.0012	0.0012
$\bar{\varepsilon}^{V}_{\sigma,mean}$	1.449	0.995	0.751	0.619	0.531
$\bar{\varepsilon}^{\theta}_{\mu,mean}$	0.362	0.213	0.152	0.123	0.107
$\bar{\varepsilon}^{\theta}_{\sigma,mean}$	2.685	1.921	1.511	1.356	1.204
$\bar{\varepsilon}^{P}_{\mu,mean}$	0.916	0.606	0.477	0.415	0.375
$\bar{\varepsilon}^{P}_{\sigma,mean}$	2.506	1.659	1.203	0.951	0.805
$\bar{\varepsilon}^{Q}_{\mu,mean}$	1.366	0.953	0.823	0.810	0.827
$\bar{\varepsilon}^{Q}_{\sigma,mean}$	2.343	1.690	1.356	1.181	1.083

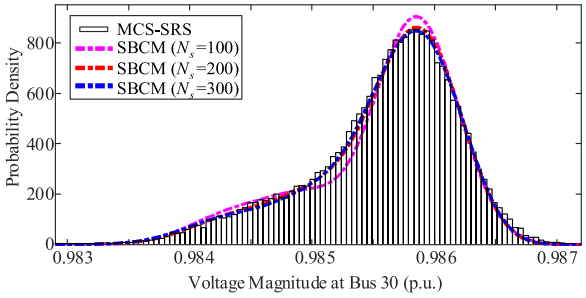

Fig. 9. Probability density curves of voltage magnitude at Bus 30.

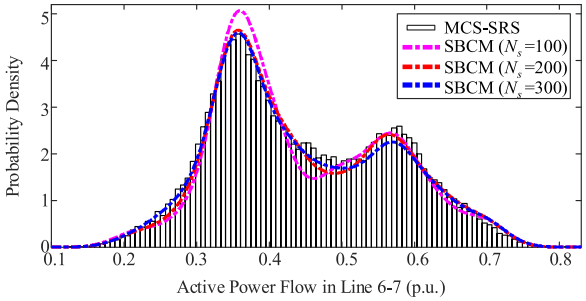

Fig. 10. Probability density curves of active power flow in line 6–7.

Table 12
Computational burden analysis of IEEE 118-bus test system (s).

Method	T_{TOTAL}	T_{SG}	T_{SD}	T_{CM}	T_{POST}
MCS-SRS	647.04	–	–	–	–
SBCM (N_s = 100)	5.35	0.12	3.42	1.79	0.02
SBCM (N_s = 300)	8.57	0.12	3.19	5.23	0.03
SBCM (N_s = 500)	11.85	0.12	2.94	8.74	0.05

Table 12 shows the computational burden of the IEEE 118-bus test system. Due to the scale of the test system, the required computation time by MCS-SRS is 647.04 s. In contrast, the proposed SBCM with 300 representative scenarios only requires 8.57 s, which is 1/75 consumed by MCS-SRS.

Compared to the computational burden of the IEEE 14-bus system in Table 8, although the number of input RVs increases dramatically in the IEEE 118-bus system, the computation time of SBCM is rising slightly. The comparison indicates that the computational burden of the proposed SBCM is mainly depended on scenario size and less sensitive to the dimensionality of uncertainties.

6. Conclusion

In this paper, a novel analytical method for PLF analysis is proposed. This method can flexibly consider various kinds of input RVs and their correlations, especially the nonlinear correlations among the RES outputs. The performance of the method is validated by the numerical experiments on the standard test systems. The results show that the proposed method achieves high accuracy in estimating statistical moments and multimodal probability distributions of desired outputs. Meanwhile, this method requires less computation time and is less affected by the dimensionality of input variables. These merits make the method suitable for solving the PLF problem of large-scale power systems.

The proposed method can be used to solve uncertainty problems such as probabilistic risk assessment, probability optimal power flow, and network planning. Future work of the proposed method includes searching for an adaptive scheme to determine the optimal number of representative scenarios.

Conflict of interest

The authors declare that they have no known competing financial interests or personal relationships that could have appeared to influence the work reported in this paper.

CRediT authorship contribution statement

Chenxu Wang: Conceptualization, Methodology, Software, Writing - original draft. **Chengxi Liu:** Writing - review & editing. **Fei Tang:** Project administration. **Dichen Liu:** Supervision. **Yixi Zhou:** Visualization.

Acknowledgment

This work was supported by the Science and Technology Project of State Grid Corporation of China (SGHBJY00PSJS1800038).

References

[1] B. Borkowska, Probabilistic load flow, IEEE Trans. Power App. Syst. PAS-93 (3) (1974) 752–759.
[2] B.R. Prusty, D. Jena, A critical review on probabilistic load flow studies in uncertainty constrained power systems with photovoltaic generation and a new approach, Renew. Sustain. Energy Rev. 69 (2017) 1286–1302.
[3] S. Conti, S. Raiti, Probabilistic load flow using Monte Carlo techniques for distribution networks with photovoltaic generators, Sol. Energy 81 (12) (2007) 1473–1481.
[4] M. Hajian, W.D. Rosehart, H. Zareipour, Probabilistic power flow by Monte Carlo simulation with latin supercube sampling, IEEE Trans. Power Syst. 28 (2) (2013) 1550–1559.
[5] D. Cai, D. Shi, J. Chen, Probabilistic load flow with correlated input random variables using uniform design sampling, Electr. Power Energy Syst. 63 (2014) 105–112.
[6] Y. Chen, J.Y. Wen, S.J. Cheng, Probabilistic load flow method based on Nataf transformation and latin hypercube sampling, IEEE Trans. Sustain. Energy 4 (2) (2013) 294–301.
[7] Y. Liu, S. Gao, H. Cui, L. Yu, Probabilistic load flow considering correlations of input variables following arbitrary distributions, Electr. Power Syst. Res. 140 (2016) 354–362.
[8] M. Abdelaziz, Gpu-opencl accelerated probabilistic power flow analysis using Monte-Carlo simulation, Electr. Power Syst. Res. 147 (2017) 70–72.
[9] P. Zhang, S.T. Lee, Probabilistic load flow computation using the method of combined cumulants and Gram-Charlier expansion, IEEE Trans. Power Syst. 19 (February (1)) (2004) 676–682.
[10] F.J. Ruiz-Rodriguez, J.C. Hernandez, F. Jurado, Probabilistic load flow for photovoltaic distributed generation using the Cornish-Fisher expansion, Electr. Power Syst. Res. 89 (2012) 129–138.
[11] M. Fan, V. Vittal, G.T. Heydt, R. Ayyanar, Probabilistic power flow studies for transmission systems with photovoltaic generation using cumulants, IEEE Trans. Power Syst. 27 (4) (2012) 2251–2261.
[12] T. Williams, C. Crawford, Probabilistic load flow modeling comparing maximum entropy and Gram-Charlier probability density function reconstructions, IEEE Trans. Power Syst. 28 (1) (2013) 272–280.
[13] M.T. Kenari, M.S. Sepasian, M.S. Nazar, H.A. Mohammadpour, The combined cumulants and laplace transform method for probabilistic load flow analysis, IET Gener. Transm. Dis. 11 (14) (2017) 694–704.
[14] F.J. Ruiz-Rodriguez, J.C. Hernandez, F. Jurado, Probabilistic load flow for radial distribution networks with photovoltaic generators, IET Renew. Power Gener. 6 (2) (2012) 110–121.
[15] J.C. Hernandez, F.J. Ruiz-Rodriguez, F. Jurado, Modelling and assessment of the combined technical impact of electric vehicles and photovoltaic generation in radial distribution systems, Energy 141 (15) (2017) 316–332.
[16] C. Liu, K. Sun, B. Wang, W. Ju, Probabilistic power flow analysis using multidimensional holomorphic embedding and generalized cumulants, IEEE Trans. Power Syst. 33 (6) (2018) 7132–7142.
[17] B.R. Prusty, D. Jena, Combined cumulant and gaussian mixture approximation for correlated probabilistic load flow studies: a new approach, CSEE J. Power Energy Syst. 2 (2) (2016) 71–78.
[18] B.R. Prusty, D. Jena, A sensitivity matrix-based temperature augmented probabilistic load flow study, IEEE Trans. Ind. Appl. 53 (3) (2017) 2506–2516.
[19] Y. Wang, N. Zhang, Q. Chen, J. Yang, C. Kang, J. Huang, Dependent discrete convolution based probabilistic load flow for the active distribution system, IEEE Trans. Sustain. Energy 8 (3) (2017) 1000–1009.
[20] C.-L. Su, Probabilistic load flow computation using point estimate method, IEEE Trans. Power Syst. 20 (4) (2005) 1843–1851.
[21] C. Chen, W. Wu, B. Zhang, H. Sun, Correlated probabilistic load flow using a point estimate method with nataf transformation, Int. J. Electr. Power Energy Syst. 65 (2015) 325–333.
[22] H. Wu, Y. Zhou, S. Dong, Y. Song, Probabilistic load flow based on generalized polynomial chaos, IEEE Trans. Power Syst. 32 (1) (2017) 820–821.
[23] F. Ni, P.H. Nguyen, J.F. Cobben, Basis-adaptive sparse polynomial chaos expansion for probabilistic power flow, IEEE Trans. Power Syst. 32 (1) (2017) 694–704.
[24] H. Sheng, X. Wang, Applying polynomial chaos expansion to assess probabilistic available delivery capability for distribution networks with renewables, IEEE Trans. Power Syst. 33 (6) (2018) 6726–6735.
[25] X. Sun, Q. Tu, J. Chen, C. Zhang, X. Duan, Probabilistic load flow calculation based on sparse polynomial chaos expansion, IET Gener. Transm. Distrib. 12 (11) (2018) 2735–2744.
[26] J. Xu, X. Yi, Y. Sun, T. Lan, H. Sun. Stochastic optimal scheduling based on scenario analysis for wind farms, IEEE Trans. Sustain. Energy 8 (4) (2017) 1548–1559.
[27] B.R. Prusty, D. Jena, An over-limit risk assessment of PV integrated power system using probabilistic load flow based on multi-time instant uncertainty modeling, Renew. Energy 116 (2018) 367–383.
[28] X. Wang, H.D. Chiang, J. Wang, et al., Long-term stability analysis of power systems with wind power based on stochastic differential equations: model development and foundations, IEEE Trans. Sustain. Energy 6 (4) (2015) 1534–1542.
[29] Z.M. Salameh, B.S. Borowy, A.R.A. Amin, Photovoltaic module-site matching based on the capacity factors, IEEE Trans. Energy Convers. 10 (2) (1995) 326–332.
[30] G. Papaefthymiou, D. Kurowicka, Using copulas for modeling stochastic dependence in power system uncertainty analysis, IEEE Trans. Power Syst. 24 (1) (2009) 40–49.
[31] D. Cai, D. Shi, J. Chen, Probabilistic load flow computation using copula and latin hypercube sampling, IET Gener. Transm. Distrib. 8 (9) (2014) 1539–1549.
[32] S. Xie, Z. Hu, D. Zhou, Y. Li, S. Kong, W. Lin, et al., Multi-objective active distribution networks expansion planning by scenario-based stochastic programming considering uncertain and random weight of network, Appl. Energy 219 (2018) 207–225.
[33] H. Heitsch, W. Romisch, Scenario reduction algorithms in stochastic programming, Comput. Algorithms Appl. 24 (2003) 187–206.
[34] Y. Wang, N. Zhang, C. Kang, M. Miao, R. Shi, Q. Xia, An efficient approach to power system uncertainty analysis with high-dimensional dependencies, IEEE Trans. Power Syst. 33 (3) (2018) 2984–2994.
[35] Wikipedia https://en.wikipedia.org/wiki/Law_of_total_probability.
[36] P. McCullagh, Tensor Methods in Statistics, Chapman and Hall, London, 1987.
[37] R.D. Zimmerman, C.E. Murillo-Sánchez, R.J. Thomas, Matpower: steady-state operations, planning and analysis tools for power systems research and education, IEEE Trans. Power Syst. 26 (1) (2011) 12–19.
[38] R.A. González-Fernández, A.M.L. da Silva, L.C. Resende, M.T. Schilling, Composite systems reliability evaluation based on Monte Carlo simulation and cross-entropy methods, IEEE Trans. Power Syst. 28 (4) (2013) 4598–4606.
[39] A.M.L. da Silva, A.M. de Castro, Risk assessment in probabilistic load flow via Monte Carlo simulation and cross-entropy method, IEEE Trans. Power Syst. 34 (2) (2019) 1193–1202.